ARTICLES
PUBLISHED ONLINE: 22 JANUARY 2012 | DOI: 10.1038/NPHYS2208
nature physics

Chiral superconductivity from repulsive interactions in doped graphene

Rahul Nandkishore[1], L. S. Levitov[1] and A. V. Chubukov[2]*

Chiral superconductivity, which breaks time-reversal symmetry, can exhibit a wealth of fascinating properties that are highly sought after for nanoscience applications. We identify doped graphene monolayer as a system where chiral superconductivity can be realized. In this material, a unique situation arises at a doping where the Fermi surface is nested and the density of states is singular. In this regime, *d*-wave superconductivity can emerge from repulsive electron–electron interactions. Using a renormalization group method, we argue that superconductivity dominates over all competing orders for generic weak repulsive interactions. Superconductivity develops simultaneously in two degenerate *d*-wave pairing channels. We argue that the resulting superconducting state is of chiral type, with the phase of the superconducting order parameter winding by 4π around the Fermi surface. Realization of this state in doped graphene will prove that superconductivity can emerge from electron–electron repulsion, and will open the door to applications of chiral superconductivity.

The simplicity of the electronic properties of graphene[1] is both a blessing and a curse. On one hand, it singles out graphene as a material of choice for applications. On the other hand, the difficulty of modifying the electronic spectrum severely limits the available functionality[2]. However, the effects of electron–electron interactions gain more prominence when the electron concentration is adjusted so that the carrier dispersion at the Fermi level becomes quadratic rather than linear. This is the case in graphene bilayer at the Dirac point, where a variety of new correlated states have been predicted[3]. This is also the case in graphene monolayer doped to the saddle point, where the density of states (DOS) has a Van Hove singularity. Although a number of interesting states have been considered in this system[4–8], the competition between these states is at present poorly understood. In this Article, we argue that generic repulsive interactions favour a superconducting $d+id$ state with the $d_{(x\pm iy)^2}$ gap structure and broken time-reversal symmetry (TRS). Our renormalization group analysis indicates that superconductivity dominates over competing density-wave orders, and also indicates that interactions select the chiral $d+id$ state over TRS-preserving d-wave states.

Chiral superconductors are interesting because they feature pairing gaps that wind in phase around the Fermi surface in multiples of 2π, breaking the TRS and exhibiting many other fascinating properties[9–11]. The non-trivial topology of the $d+id$ state is analogous to that studied in other systems with chiral pairing, such as the two-dimensional ^{3}He (ref. 9) and the fractional quantum Hall state at 5/2 filling[12,13]. Interest in chiral superconductivity has intensified greatly in the past few years with the advent of topological superconductivity[14–16]. The non-trivial topological properties manifest themselves in exceptionally rich phenomenology, in particular the Majorana states in vortex defects[17] and the gapless modes bound to the edge by Andreev scattering that can carry quantized particle current and spin current[18]. Similar phenomena have been predicted for the hypothetical $d+id$ state in cuprate superconductors[19–22] and other chiral superconducting states[23,24].

The search for solid-state realization of chiral superconductivity has a long history. Spin-triplet p-wave chiral superconductivity ($p_x \pm ip_y$ state) has probably been found in Sr_2RuO_4 (ref. 25), which represents an analogue of superfluid ^{3}He (ref. 9), but the spin-singlet $d+id$ state has not yet been observed experimentally. Such a state was once proposed as a candidate state for high-T_c cuprate superconductors[19], but later gave way to a more conventional TRS-preserving d-wave state. The key difficulty in realizing a $d+id$ state is that the interactions that favour a d-wave state usually have strong momentum dependence and hence distinguish between $d_{x^2-y^2}$ and d_{xy} pairing. However, in graphene the $d_{x^2-y^2}$ and d_{xy} pairing channels are degenerate by symmetry[4,26], opening the door to formation of a $d+id$ superconducting state.

How can superconductivity be induced in graphene? Existing proposals for superconductivity in undoped graphene rely on the conventional phonon-mediated BCS mechanism[27], which leads to an s-wave superconductivity with low T_c values for realistic carrier densities owing to the vanishing density of states of relativistic particles. However, there is an alternative route to superconductivity, wherein repulsive microscopic interactions give rise to attraction in a d-wave channel[28]. This alternative route becomes viable when graphene is doped to the M point of the Brillouin zone corresponding to 3/8 or 5/8 filling of the π band (pristine graphene corresponds to 1/2 filling). At this filling factor, a logarithmic Van Hove singularity originates from three inequivalent saddle points, and the Fermi surface also exhibits a high degree of nesting, forming a perfect hexagon when third-neighbour (and higher) hopping effects are neglected[1,4] (Fig. 1). The combination of a singular DOS and a near-nested Fermi surface strongly enhances the effect of interactions[29–31], allowing non-trivial phases to emerge at relatively high temperatures, even if interactions are weak compared with the fermionic bandwidth W. Relevant doping levels were recently achieved experimentally using calcium and potassium dopants[32]. Also, a new technique[33] that employs ionic liquids as gate dielectrics allows high levels of doping to be reached without introducing chemical disorder.

[1]Department of Physics, Massachusetts Institute of Technology, Cambridge, Massachusetts 02139, USA, [2]Department of Physics, University of Wisconsin-Madison, Madison, Wisconsin 53706, USA. *e-mail: chubukov@physics.wisc.edu.

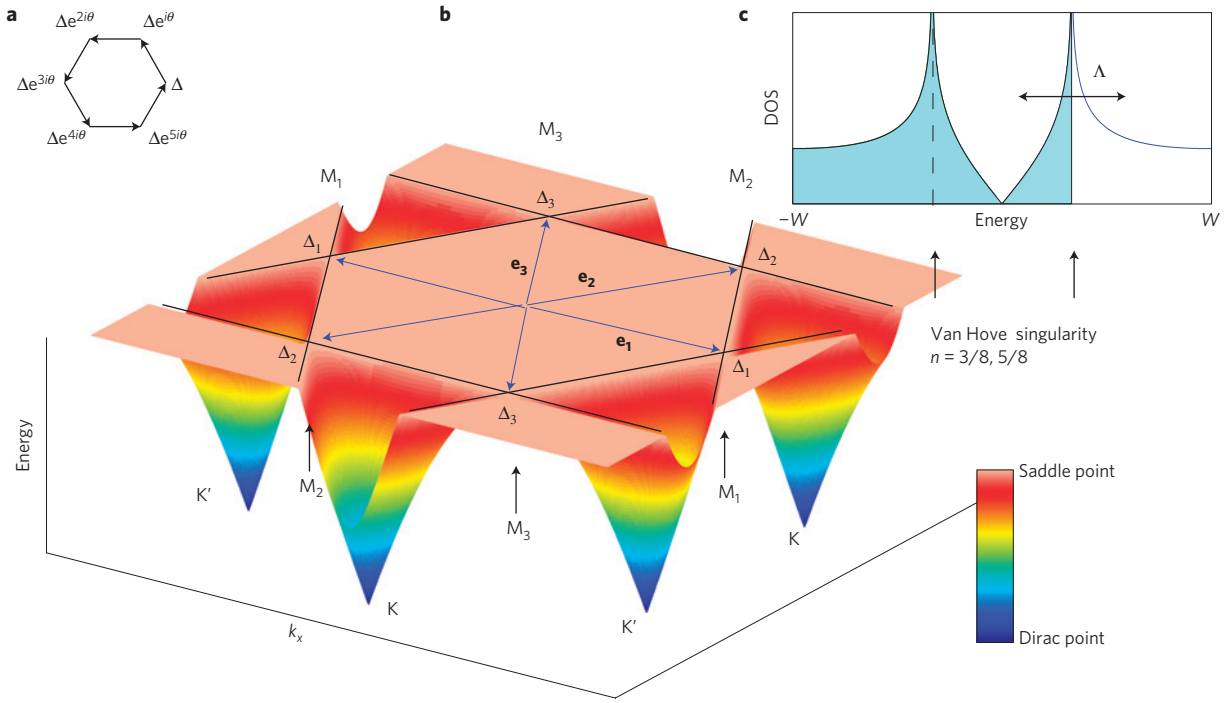

Figure 1 | Chiral superconductivity arises when graphene is doped to the Van Hove singularity at the saddle point (M points of the Brillouin zone). **a**, $d+id$ pairing exhibiting phase winding around the hexagonal Fermi surface, which breaks TRS and parity ($\theta = 2\pi/3$). **b**, Conduction band for monolayer graphene[1]. At 5/8 filling of the π band, the Fermi surface is hexagonal, and the DOS is logarithmically divergent (**c**) at three inequivalent saddle points of the dispersion M_i ($i = 1, 2, 3$). Their locations are given by $\pm\mathbf{e}_i$, where $2\mathbf{e}_i$ is a reciprocal lattice vector. The singular DOS strongly enhances the effect of interactions, driving the system into a chiral superconducting state (**a**). As the Fermi surface is nested, superconductivity competes with density-wave instabilities, and a full renormalization group treatment is required to establish the dominance of superconductivity. A hexagonal Fermi surface and log divergent density of states also arise at 3/8 filling, giving rise to analagous physics.

Competing orders

In systems with near-nested Fermi surface, superconductivity has to compete with charge-density-wave (CDW) and spin-density-wave (SDW) instabilities[34]. At the first glance, it may seem that a system with repulsive interactions should develop a density-wave order rather than become a superconductor. However, to analyse this properly, one needs to know the susceptibilities to the various orders at a relatively small energy, E_0, at which the order actually develops. The couplings at E_0 generally differ from their bare values because of renormalizations by fermions with energies between E_0 and W. At weak coupling, these renormalizations are well captured by the renormalization group technique.

Interacting fermions with a nested Fermi surface and logarithmically divergent DOS have previously been studied on the square lattice using renormalization group methods[29–31,34], where SDW fluctuations were argued to stimulate superconductivity. The analysis also revealed near degeneracy between superconductivity and SDW orders. The competition between these orders is decided by a subtle interplay between deviations from perfect nesting, which favour superconductivity, and subleading terms in the renormalization group flow, which favour SDW. In contrast, the renormalization group procedure on the honeycomb lattice unambiguously selects superconductivity at leading order, allowing us to safely neglect subleading terms. The difference arises because the honeycomb lattice contains three saddle points, whereas the square lattice has only two, and the extra saddle point tips the balance seen on the square lattice between magnetism and superconductivity decisively in favour of superconductivity. A similar tipping of a balance between superconductivity and SDW in favour of superconductivity has been found in renormalization group studies of Fe-pnictide superconductors[35,36].

In previous works on graphene at the M point, various instabilities were analysed using the random-phase approximation (RPA) and mean-field theory. Ref. 4 considered the instability to d-wave superconductivity, ref. 5 considered a charge 'Pomeranchuk' instability to a metallic phase breaking lattice rotation symmetry, and refs 6–8 considered a SDW instability to an insulating phase. Within the framework of mean-field theory, used in the above works, all of these phases are legitimate potential instabilities of the system. However, clearly graphene at the M point cannot be simultaneously superconducting, metallic and insulating. The renormalization group analysis treats all competing orders on an equal footing, and predicts that the dominant weak coupling instability is to superconductivity, for any choice of repulsive interactions, even for perfect nesting. Further, the Ginzburg–Landau theory constructed near the renormalization group fixed point favours the $d+id$ state.

The model

We follow the procedure developed for the square lattice[34] and construct a patch renormalization group that considers only fermions near three saddle points, which dominate the DOS. There are four distinct interactions in the low-energy theory, involving two-particle scattering between different patches, as shown in Fig. 2.

The system is described by the low-energy theory

$$\mathcal{L} = \sum_{\alpha=1}^{3} \psi_\alpha^\dagger (\partial_\tau - \epsilon_{\mathbf{k}} + \mu)\psi_\alpha - \frac{1}{2} g_4 \psi_\alpha^\dagger \psi_\alpha^\dagger \psi_\alpha \psi_\alpha - \sum_{\alpha \neq \beta} \frac{1}{2}\left[g_1 \psi_\alpha^\dagger \psi_\beta^\dagger \psi_\alpha \psi_\beta + g_2 \psi_\alpha^\dagger \psi_\beta^\dagger \psi_\beta \psi_\alpha + g_3 \psi_\alpha^\dagger \psi_\alpha^\dagger \psi_\beta \psi_\beta \right] \quad (1)$$

where summation is over patch labels $\alpha, \beta = M_1, M_2, M_3$. A spin sum is implicit in the above expression, with the spin structure for each of the four terms being $\gamma, \delta, \delta, \gamma$, where γ and δ label the spin up and down states. Here $\epsilon_{\mathbf{k}}$ is the tight binding dispersion, expanded

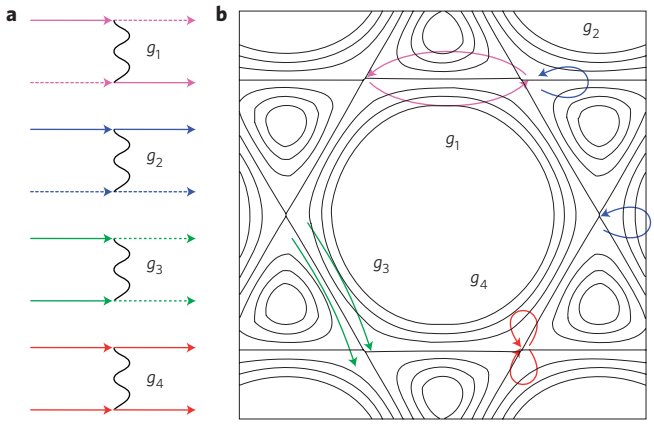

Figure 2 | Possible interactions in the patch model. a, Feynman diagrams representing allowed two-particle scattering processes among different patches (equation (1)). Solid and dashed lines represent fermions on different patches, whereas wavy lines represent interactions. **b**, Pictorial representation of these scattering processes, superimposed on a contour plot of the energy dispersion. Each scattering process comes in three flavours, according to the patches involved. However, it follows by symmetry that the scattering amplitudes are independent of the patches involved, and therefore we suppress the flavour labels.

up to quadratic terms about each saddle point. For example, near point M_1, the tight-binding model[37] predicts dispersion $\epsilon_{\mathbf{k}} = 2\pi^2 a^2 t((\delta k_x)^2 - \sqrt{3}\delta k_x \delta k_y + O((\delta k)^4))$, where t is the nearest-neighbour hopping, a is the lattice constant and $\delta\mathbf{k} = \mathbf{k} - \mathbf{k}_{M_1}$. The chemical potential value $\mu = 0$ describes a system doped exactly to the saddle point. We note that whereas the existence of saddle points is a topological property of the Fermi surface and is robust to arbitrarily long-range hopping, the Fermi surface nesting is spoilt by third-neighbour (and higher) hopping effects[1,4]. Inequivalent saddle points are connected by a nesting vector $Q_{\alpha\beta} = \mathbf{e}_\alpha - \mathbf{e}_\beta$ (Fig. 1). The short-range interaction model, used in our analysis, is expected to provide a good approximation under the conditions of metallic screening arising due to the states near the Fermi surface. The screening generally depends on the level of doping relative to the M point, introducing some uncertainty into the bare values for the interactions. However, we will show that precise knowledge of these bare values is not required to determine the final state.

The patch structure of the interactions is restricted by momentum conservation, which allows only the four interactions in equation (1). The umklapp interaction g_3 is allowed, because it conserves momentum modulo a reciprocal lattice vector. All four interactions in equation (1) are marginal at tree level, but acquire logarithmic corrections in perturbation theory. These logarithmic corrections come from energy scales $E < \Lambda$, where $\Lambda \approx t$ is the energy scale at which higher order corrections to the dispersion become important.

Logarithmic divergences in perturbation theory analysis indicate that the problem is well suited to study using a renormalization group technique. The building blocks of the renormalization group are the susceptibilities in the particle–particle and particle–hole channels, $\Pi_{\rm pp}$ and $\Pi_{\rm ph}$, evaluated respectively at momentum transfer zero and at momentum transfer $Q_{\alpha\neq\beta}$ between points M_α and M_β. Similarly to ref. 34, we have

$$\Pi_{\rm pp}(0) = \frac{\nu_0}{4}\ln\frac{\Lambda}{\max(T,\mu)}\ln\frac{\Lambda}{T},$$

$$\Pi_{\rm ph}(Q_{\alpha\neq\beta}) = \frac{\nu_0}{4}\ln\frac{\Lambda}{\max(T,\mu)}\ln\frac{\Lambda}{\max(T,\mu,t_3)}$$

and $\Pi_{\rm ph}(0)$, $\Pi_{\rm pp}(Q_{\alpha\neq\beta}) = \nu_0\ln(\Lambda/\max(T,\mu))$, where Λ is our ultraviolet cutoff (Fig. 1) and T is the temperature. The density of states at a saddle point is $\nu_0\ln(\Lambda/\max(T,\mu))$ per spin projection. The second log factor in $\Pi_{pp}(0)$ arises in a conventional way owing to the divergence in the Cooper channel. The second log factor in $\Pi_{\rm ph}(Q_{\alpha\neq\beta})$ arises from nesting of the Fermi surface, and is cut in the infrared by any term that spoils the nesting, such as third-neighbour hopping t_3 or doping μ (ref. 4). At weak coupling the Cooper log is large, and we assume that $\max(t_3,\mu) \ll \Lambda$ so that the nesting log is also large. In this limit, $\Pi_{pp}(0)$ and $\Pi_{\rm ph}(Q)$ are parametrically larger than $\Pi_{\rm ph}(0)$ and $\Pi_{\rm pp}(Q)$, so that the renormalization group is dominated by the double log divergent susceptibilities.

Renormalization group equations

The renormalization group equations are obtained by extending the approach developed for the square lattice problem[31] to a number of patches $n > 2$. The number of patches matters only in diagrams with zero net momentum in fermion loops, as it is only there that we get summation over fermion flavours inside the loop. The only zero-momentum loop with a $\log^2$ divergence is in the Cooper channel. Moreover, only the g_3 interaction changes the patch label of a Cooper pair, therefore, the number of patches affects only diagrams where two g_3 interactions are combined in the Cooper channel. With logarithmic accuracy, using $y = \Pi_{\rm pp}(\mathbf{k}=0,E) = (\nu_0/4)\ln^2(\Lambda/E)$ as the renormalization group time, we obtain the β-functions

$$\frac{{\rm d}g_1}{{\rm d}y} = 2d_1 g_1(g_2 - g_1), \quad \frac{{\rm d}g_2}{{\rm d}y} = d_1(g_2^2 + g_3^2)$$
$$\frac{{\rm d}g_3}{{\rm d}y} = -(n-2)g_3^2 - 2g_3 g_4 + 2d_1 g_3(2g_2 - g_1), \qquad (2)$$
$$\frac{{\rm d}g_4}{{\rm d}y} = -(n-1)g_3^2 - g_4^2$$

Here $d_1(y) = {\rm d}\Pi_{\rm ph}(Q)/{\rm d}y \approx \Pi_{\rm ph}(Q)/\Pi_{\rm pp}(0)$ is the 'nesting parameter'[31,34]. This quantity equals one in the perfectly nested limit. For non-perfect nesting, $d_1(y)$ has the asymptotic forms $d_1(y=0) = 1$, $d_1(y \gg 1) = \ln|\Lambda/t_3|/\sqrt{y}$, and interpolates smoothly in between. Because the renormalization group equations flow to strong coupling at a finite scale $y_{\rm c}$, we treat $0 < d_1(y_{\rm c}) < 1$ as a parameter in our analysis.

The β-functions, equation (2), reproduce the two-patch renormalization group from ref. 31 when we take $n = 2$ and neglect subleading $O(\log)$ divergent terms ($d_{2,3}(y)$ from ref. 31), and also reproduce for $n = 2$ the renormalization group equations for the Fe-pnictides[35]. Graphene near the Van Hove singularity, however, is described by $n = 3$.

We note from inspection of equation (2) that g_1, g_2 and g_3 must stay positive (repulsive) if they start out positive. This follows because the β-function for g_2 is positive definite, and the β-functions for g_1 and g_3 vanish as the respective couplings go to zero. However, g_4 decreases under the renormalization group, eventually changing sign and becoming negative. As we will see, $g_3 - g_4$ becomes large and positive under the renormalization group, driving an instability to a superconducting phase. However, the positive g_3 coupling penalizes s-wave superconductivity, so pairing occurs in a higher angular momentum (d-wave) channel.

We integrate our renormalization group equations with $n = 3$, starting from $g_i = g_0 = 0.1$ (these values are chosen for illustration) and modelling d_1 as $d_1(y) = 1/\sqrt{1+y}$. The results are plotted in Fig. 3. Similar results are obtained if we just treat d_1 as a constant. The couplings diverge at a scale $y_{\rm c} \sim 1/g_0$, corresponding to a critical temperature and ordering energy scale

$$T_{\rm c}, E_0 \sim \Lambda\exp(-A/\sqrt{g_0\nu_0}) \qquad (3)$$

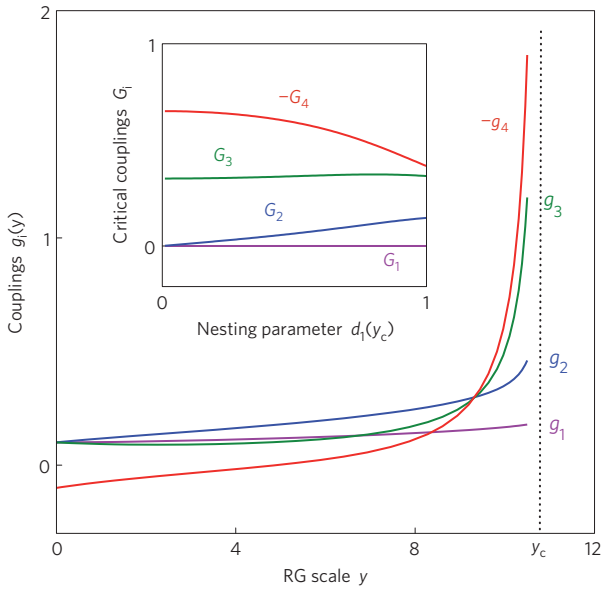

Figure 3 | Flow of couplings with renormalization group scale y, starting from repulsive interactions. Note that the coupling g_4 changes sign and becomes attractive, leading to a (superconducting) instability at the energy scale y_c (equation (3)). Inset: Critical couplings G_i (equation (4)) near y_c as a function of the nesting parameter at the ordering energy scale, $d_1(y_c)$. The dominance of superconductivity over spin-density-wave order arises because $-G_4 > G_2$ for all values of $d_1(y_c)$. The renormalization group flow is obtained by numerical integration of (2) with the initial conditions $g_i(0) = 0.1$ and modelling the nesting parameter as $d_1(y) = 1/\sqrt{1+y}$. The qualitative features of the flow are insensitive to the initial conditions and to how we model d_1. The critical couplings (inset) are universal and independent of the initial conditions.

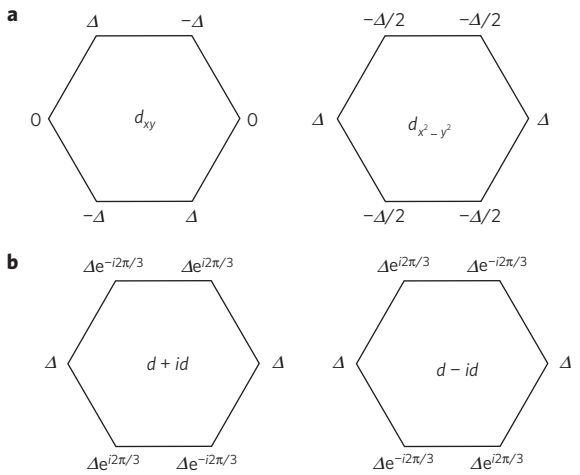

Figure 4 | Possible superconducting orders that could develop at the M point. a, A $d_{x^2-y^2}$ or d_{xy} state would be realized if $K_2 < 0$ in the Landau expression for the free energy, equation (10). **b**, The $d_{x^2-y^2}$ and d_{xy} orders can co-exist if $K_2 > 0$ in equation (10). A microscopic calculation indicates that the states (**b**) have lower free energy.

Here A is a non-universal number that depends on how we model $d_1(y)$. For $d_1 = 1$ (perfect nesting, corresponding to zero third-neighbour hopping t_3), we obtain $A = 1.5$. An RPA-type estimate of g_0 is outlined in the Supplementary Information. Although T_c and E_0 are exponentially sensitive to g_0, thus introducing a considerable uncertainty to our estimate, a strong enhancement of characteristic energy scales relative to the BCS result is evident from equation (3).

A similar $\sqrt{g_0}$ dependence arises in the treatment of colour superconductivity[38] and in the analysis of the pairing near quantum-critical points in 3D (ref. 39). It results in a T_c that is strongly enhanced compared with the standard BCS result, $T_c \sim \exp(-A'/g_0\nu_0)$. It should be noted that the enhancement of T_c in equation (3) arises from weak-coupling physics. It is distinct from the high-T_c superconductivity that could arise if the microscopic interactions were strong[26,40–42].

Returning to our renormalization group analysis, we note that near the instability threshold, $g_1, g_2, g_3 \to \infty$ and $g_4 \to -\infty$, with $-g_4 > g_3 > g_2 > g_1$. This observation may be made precise by noting that close to y_c, the interactions scale as

$$g_i(y) \approx \frac{G_i}{y_c - y} \tag{4}$$

Substituting into equation (2), we obtain a set of polynomial equations, which may be solved for the coefficients G_i as a function of $d_1(y_c)$. The solution is plotted in the inset of Fig. 3. Note that $-G_4 > G_3 > G_2 > G_1$ for all values of $d_1(y_c)$ satisfying $0 \le d_1(y_c) \le 1$. We have verified that any choice of repulsive bare couplings leads to the same limiting trajectory (see Supplementary Information).

Susceptibilities

We now investigate the instabilities of the system by evaluating the susceptibilities χ for various types of order. To analyse the superconducting instability, we introduce infinitesimal test vertices corresponding to particle–particle pairing into the action, $\mathcal{L} = \mathcal{L}_0 + \delta\mathcal{L}$, where $\mathcal{L}_0$ is given by equation (1) and

$$\delta\mathcal{L} = \sum_{\alpha=1}^{3} \tilde{\Delta}_\alpha \psi^\dagger_{\alpha,\uparrow} \psi^\dagger_{\alpha,\downarrow} + \tilde{\Delta}^*_\alpha \psi_{\alpha,\uparrow} \psi_{\alpha,\downarrow}$$

one test vertex for each patch. The renormalization of the test vertices is governed by the equation[31]

$$\frac{\partial}{\partial y}\begin{bmatrix}\tilde{\Delta}_1\\ \tilde{\Delta}_2\\ \tilde{\Delta}_3\end{bmatrix} = -2\begin{bmatrix}g_4 & g_3 & g_3\\ g_3 & g_4 & g_3\\ g_3 & g_3 & g_4\end{bmatrix}\begin{bmatrix}\tilde{\Delta}_1\\ \tilde{\Delta}_2\\ \tilde{\Delta}_3\end{bmatrix} \tag{5}$$

which can be diagonalized by transforming to the eigenvector basis

$$\tilde{\Delta}_a = \frac{\tilde{\Delta}}{\sqrt{2}}(0,1,-1), \quad \tilde{\Delta}_b = \sqrt{\frac{2}{3}}\tilde{\Delta}\left(1,-\frac{1}{2},-\frac{1}{2}\right) \tag{6}$$

$$\tilde{\Delta}_c = \frac{\tilde{\Delta}}{\sqrt{3}}(1,1,1) \tag{7}$$

Here $\tilde{\Delta}_c$ is an s-wave order, whereas $\tilde{\Delta}_a$ and $\tilde{\Delta}_b$ correspond to order parameters that vary around the Fermi surface as $\tilde{\Delta}\cos(2\varphi)$ and $\tilde{\Delta}\sin(2\varphi)$, where φ is the angle to the x axis (Fig. 4). Such a dependence describes d-wave superconducting orders (SCd), as the gap changes sign four times along the Fermi surface. In 2D notation, the two order parameters $\tilde{\Delta}_a$ and $\tilde{\Delta}_b$ correspond to d_{xy} and $d_{x^2-y^2}$ superconducting orders respectively.

Notably, we find that the s-wave vertex $\tilde{\Delta}_c$, equation (7), has a negative eigenvalue and is suppressed under renormalization group flow (equation (5)). This is to be expected, given that we started out with repulsive microscopic interactions. At the same time, the d-wave orders $\tilde{\Delta}_a$ and $\tilde{\Delta}_b$ have the (identical) eigenvalue $g_3 - g_4$, which may be negative at the bare level but becomes positive under the renormalization group, indicating an instability in the d-wave channel. We solve equation (5) for the d-wave orders, by

substituting the scaling form of the interactions (equation (4)), and find that the d-wave susceptibility diverges near y_c as

$$\chi_{\mathrm{SCd}}(y) = \frac{\tilde{\Delta}_{a,b}(y)}{\tilde{\Delta}_{a,b}(0)} \sim (y_c - y)^{2(G_4 - G_3)} \tag{8}$$

where we recall, $G_3 - G_4 > 0$.

The divergence of the SCd susceptibility indicates an instability to d-wave superconductivity under the renormalization group, with the $\tilde{\Delta}\cos(2\varphi)$ and $\tilde{\Delta}\sin(2\varphi)$ order parameters having identical susceptibility. The degeneracy of the two d-wave orders is guaranteed, because the $d_{x^2-y^2}$ and d_{xy} functions belong to the same 2D irreducible representation of the lattice point group[4,26]. However, this does not guarantee that d-wave superconductivity will develop, because the SCd instability must compete against the tendency for density-wave formation.

To investigate density-wave formation, we introduce test vertices representing pairing of particles with holes on a different patch. The particles and holes may pair in the charge channel, forming CDW, or in the spin channel, forming SDW. We compute the renormalization of the pairing vertices under the renormalization group, and find that the CDW vertex is suppressed by interactions, but the SDW vertex $\tilde{\Delta}_{\mathrm{SDW}}$ is enhanced, similar to ref. 31. The SDW susceptibility χ_{SDW} diverges near y_c as

$$\chi_{\mathrm{SDW}} = \frac{\tilde{\Delta}_{\mathrm{SDW}}(y)}{\tilde{\Delta}_{\mathrm{SDW}}(0)} \sim (y_c - y)^{-2(G_3+G_2)d_1(y_c)} \tag{9}$$

This describes a potential instability towards SDW formation, which will compete with the SCd instability. The SDW instability arises provided there is at least partial nesting (that is, the nesting parameter $d_1(y_c) \neq 0$). However, as $-G_4 > G_2$ for all $0 \leq d_1(y_c) \leq 1$ (Fig. 3 inset), it follows from comparison of equations (9) and (8) that the SCd susceptibility diverges faster than the SDW susceptibility, for all values of nesting. At perfect nesting ($d_1 = 1$), the SCd susceptibility diverges as $(y_c - y)^{-1.5}$, whereas the SDW susceptibility diverges only as $(y_c - y)^{-1}$. As we move away from perfect nesting, the SCd susceptibility diverges faster, and the SDW susceptibility diverges more slowly, so that SCd is the leading instability for all values of nesting, within validity of the renormalization group. This is in contrast to the square lattice[31], where at perfect nesting the SDW and SCd instabilities have the same exponent under the renormalization group, with subleading terms lifting the degeneracy in favour of SDW, which is in turn overtaken by SCd at some $d_1 < 1$.

We also considered the phonon-mediated attraction in the pairing channel. This interaction could induce s-wave superconductivity provided that it overwhelms the electronic repulsion in the s-wave channel at the Debye frequency scale, $\omega_D < \Lambda$. In our renormalization group flow, the s-wave coupling $(2g(3) + g(4))$ remains positive and initially drops, in complete analogy with the McMillan regime in conventional superconductors. However, it eventually changes trend and becomes more repulsive at larger renormalization group scales. The conventional s-wave pairing mediated by phonons may occur if the initial suppression is strong enough at the renormalization group scales corresponding to ω_D. Finally, we considered the possibility of ordering in a channel exhibiting only a $\log^1$ divergence, for example the Pomeranchuk ordering. However, we found that such orders cannot compete with superconductivity (see Supplementary Information).

Competition of d-wave orders below T_c

We now investigate the competition of the $d_{x^2-y^2}$ and d_{xy} superconducting orders (equation (6)) below T_c. In this regime, the system may either develop one of these two orders, or a linear combination of the two. The ordered state that minimizes the free energy wins. The hexagonal lattice point group symmetry dictates that the free energy below T_c must take the form[43]

$$\begin{aligned} F &= \alpha(T - T_c)(|\Delta_a|^2 + |\Delta_b|^2) + K_1\left(|\Delta_a|^2 + |\Delta_b|^2\right)^2 \\ &\quad + K_2|\Delta_a^2 + \Delta_b^2|^2 + O(\Delta^6) \end{aligned} \tag{10}$$

with $K_1 > 0$. This free energy allows for two possible superconducting phases. If $K_2 < 0$ then a $d_{x^2-y^2}$ or a d_{xy} superconducting state would arise, whereas if $K_2 > 0$ then the $d_{x^2-y^2}$ and d_{xy} orders can co-exist[43]. We now calculate K_2 (an alternative but equivalent microscopic treatment is provided in the Supplementary Information).

We begin by writing the free energy as the sum of the free energy on three patches

$$F = F(\Delta_1) + F(\Delta_2) + F(\Delta_3) \tag{11}$$

where the free energy on a patch is given by the standard Landau expansion

$$F(\Delta_i) = \alpha'(T - T_c)|\Delta_i|^2 + K|\Delta_i|^4, \quad K > 0 \tag{12}$$

In this expression, it is essential to realize that Δ_1, Δ_2 and Δ_3 are not independent, but must be expressed in terms of the two parameters Δ_a and Δ_b (equation (6)). Rewriting equations (11) and (12) in terms of the two independent variables $\Delta_{a,b}$, we obtain equation (10) with $K_1 = \frac{1}{3}K > 0$ and $K_2 = \frac{1}{6}K > 0$. This implies the co-existence of $d_{x^2-y^2}$ and d_{xy} orders. Minimization of the free energy (10) with $K_2 > 0$ leads to $|\Delta_a| = |\Delta_b|$ and $\mathrm{Arg}(\Delta_a/\Delta_b) = \pi/2$. This order parameter can be rewritten as a three-component vector in the patch basis, which takes the form

$$\Delta_a \pm i\Delta_b = \Delta\left(1, \mathrm{e}^{\pm 2\pi i/3}, \mathrm{e}^{\mp 2\pi i/3}\right)$$

In this state, the superconducting gap varies around the Fermi surface as $\Delta\exp(\pm 2i\varphi)$. Such an order parameter corresponds to $d_{(x\pm iy)^2}$ (or $d + id$) superconductivity (Fig. 4), and is a spin-singlet analogue of the $p + ip$ state that has been predicted for Sr_2RuO_4.

Outlook

The robustness of $d + id$ superconductivity in the weak coupling limit, demonstrated by the above analysis, leads us to believe that graphene-based chiral superconductivity can be realized experimentally. There are several questions pertaining to the behaviour of realistic systems which should be clarified by future work. Determination of the phase structure for interactions of moderate strength and of long-range character remains an open problem, as does an accurate estimate of T_c and the role of disorder, against which d-wave superconductivity is not protected. Graphene-based $d + id$ superconductivity, if realized in experiment, will play a vital role in the development of technology designed to exploit topological superconductivity.

Received 27 June 2011; accepted 13 December 2011; published online 22 January 2012

References

1. Castro Neto, A. H., Guinea, F., Peres, N. M. R., Novoselov, K. S. & Geim, A. K. The electronic properties of graphene. *Rev. Mod. Phys.* **81,** 109–162 (2009).
2. DasSarma, S., Adam, S., Hwang, E. H. & Rossi, E. Electronic transport in two-dimensional graphene. *Rev. Mod. Phys.* **83,** 407–470 (2011).
3. Guinea, F. Viewpoint: Peeling back the layers or doubling the stakes? Calculations of bilayer graphene reveal the possibility of new electronic phases. *Physics* **3,** 1 (2010).

4. Gonzalez, J. Kohn–Luttinger superconductivity in graphene. *Phys. Rev. B* **78,** 205431 (2008).
5. Valenzuela, B. & Vozmediano, M. A. H. Pomeranchuk instability in doped graphene. *New. J. Phys.* **10,** 113009 (2008).
6. Martin, I. & Batista, C. D. Itinerant electron-driven chiral magnetic ordering and spontaneous quantum Hall effect in triangular lattice models. *Phys. Rev. Lett.* **101,** 156402 (2008).
7. Li, T. Spontaneous quantum Hall effect in quarter doped Hubbard model on honeycomb lattice and its possible realization in quarter doped graphene system. Preprint at http://arxiv.org/abs/1103.2420 (2011).
8. Makogon, D., van Gelderen, R., Roldan, R. & Morais Smith, C. Spin-density-wave instability in graphene doped near the van Hove singularity. *Phys. Rev. B* **84,** 125404 (2011).
9. Volovik, G. E. Quantized hall effect in superfluid helium-3 film. *Phys. Lett. A* **128,** 277–279 (1988).
10. Sigrist, M. & Ueda, K. Phenomenological theory of unconventional superconductivity. *Rev. Mod. Phys.* **63,** 239–311 (1991).
11. Vojta, M., Zhang, Y. & Sachdev, S. Quantum phase transitions in *d*-wave superconductors. *Phys. Rev. Lett.* **85,** 4940–4943 (2000).
12. Moore, G. & Read, N. Nonabelions in the fractional quantum hall effect. *Nucl. Phys.* **B360,** 362–396 (1991).
13. Ivanov, D. A. Non-Abelian statistics of half-quantum vortices in *p*-wave superconductors. *Phys. Rev. Lett.* **86,** 268–271 (2001).
14. Fu, L. & Kane, C. L. Superconducting proximity effect and Majorana fermions at the surface of a topological insulator. *Phys. Rev. Lett.* **100,** 096407 (2008).
15. Qi, X. L., Hughes, T., Raghu, S. & Zhang, S-C. Time-reversal-invariant topological superconductors and superfluids in two and three dimensions. *Phys. Rev. Lett.* **102,** 187001 (2009).
16. Cheng, M., Sun, K., Galitski, V. & Das Sarma, S. Stable topological superconductivity in a family of two-dimensional fermion models. *Phys. Rev. B* **81,** 024504 (2010).
17. Kopnin, N. B. & Salomaa, M. M. Mutual friction in superfluid ^{3}He: Effects of bound states in the vortex core. *Phys. Rev. B* **44,** 9667–9677 (1991).
18. Volovik, G. E. & Yakovenko, V. M. Fractional charge, spin and statistics of solitons in superfluid ^{3}He film. *J. Phys. Condens. Matter* **1,** 5263–5274 (1989).
19. Laughlin, R. B. Magnetic induction of $d_{x^2-y^2} + id_{xy}$ order in high-T_c superconductors. *Phys. Rev. Lett.* **80,** 5188–5191 (1998).
20. Volovik, G. E. On edge states in superconductors with time inversion symmetry breaking. *J. Exp. Theor. Phys. Lett.* **66,** 522–527 (1997).
21. Senthil, T., Marston, J. B. & Fisher, M. P. A. Spin quantum Hall effect in unconventional superconductors. *Phys. Rev. B* **60,** 4245–4254 (1999).
22. Horovitz, B. & Golub, A. Superconductors with broken time-reversal symmetry: Spontaneous magnetization and quantum Hall effects. *Phys. Rev. B* **68,** 214503 (2003).
23. Sato, M., Takahashi, Y. & Fujimoto, S. Non-Abelian topological orders and Majorana fermions in spin-singlet superconductors. *Phys. Rev. B* **82,** 134521 (2010).
24. Mao, L., Shi, J., Niu, Q. & Zhang, C. Superconducting phase with a chiral *f*-wave pairing symmetry and Majorana fermions induced in a hole-doped semiconductor. *Phys. Rev. Lett.* **106,** 157003 (2011).
25. Mackenzie, A. P. & Maeno, Y. The superconductivity of Sr_2RuO_4 and the physics of spin-triplet pairing. *Rev. Mod. Phys.* **75,** 657–712 (2003).
26. Black-Schaffer, A. M. & Doniach, S. Resonating valence bonds and mean-field *d*-wave superconductivity in graphite. *Phys. Rev. B* **75,** 134512 (2007).
27. Uchoa, B. & Castro Neto, A. H. Superconducting states of pure and doped graphene. *Phys. Rev. Lett.* **98,** 146801 (2007).
28. Kohn, W. & Luttinger, J. M. New mechanism for superconductivity. *Phys. Rev. Lett.* **15,** 524–526 (1965).
29. Schulz, H. J. Superconductivity and antiferromagnetism in the two-dimensional Hubbard model: Scaling theory. *Europhys. Lett.* **4,** 609–615 (1987).
30. Dzyaloshinskii, I. E. Maximal increase of the superconducting transition temperature due to the presence of van Hove singularities. *Sov. Phys. JETP* **66,** 848–854 (1987).
31. Furukawa, N., Rice, T. M. & Salmhofer, M. Truncation of a two-dimensional Fermi surface due to quasiparticle gap formation at the saddle points. *Phys. Rev. Lett.* **81,** 3195–3198 (1998).
32. McChesney, J. L. *et al.* Extended van Hove singularity and superconducting instability in doped graphene. *Phys. Rev. Lett.* **104,** 136803 (2010).
33. Ye, J. T. *et al.* Liquid-gated interface superconductivity on an atomically flat film. *Nature Mater.* **9,** 125–128 (2010).
34. LeHur, K. & Rice, T. M. Superconductivity close to the Mott state: From condensed-matter systems to superfluidity in optical lattices. *Ann. Phys.* **324,** 1452–1515 (2009).
35. Maiti, S. & Chubukov, A. V. Renormalization group flow, competing phases and the structure of superconducting gap in multiband models of iron-based superconductors. *Phys. Rev. B* **82,** 214515 (2010).
36. Thomale, R., Platt, C., Hanke, W. & Bernevig, B. A. Mechanism for explaining differences in the order parameters of FeAs-based and FeP-based pnictide superconductors. *Phys. Rev. Lett.* **106,** 187003 (2011).
37. Wallace, P. R. The band theory of graphite. *Phys. Rev.* **71,** 622–634 (1947).
38. Son, D. T. Superconductivity by long-range colour magnetic interaction in high-density quark matter. *Phys. Rev. D* **59,** 094019 (1999).
39. Moon, E. G. & Chubukov, A. V. Quantum-critical pairing with varying exponents. *J. Low Temp. Phys.* **161,** 263–281 (2010).
40. Pathak, S., Shenoy, V. B. & Baskaran, G. Possible high-temperature superconducting state with a $d + id$ pairing symmetry in doped graphene. *Phys. Rev. B* **81,** 085431 (2010).
41. Honerkamp, C. Density waves and Cooper pairing on the honeycomb lattice. *Phys. Rev. Lett.* **100,** 146404 (2008).
42. Roy, B. & Herbut, I. F. Unconventional superconductivity on honeycomb lattice: Theory of Kekule order parameter. *Phys. Rev. B* **82,** 035429 (2010).
43. Mineev, V. P. & Samokhin, K. V. *Introduction to Unconventional Superconductivity* 69 (Gordon and Breach Science Publishers, 1998).

Author contributions

R.N., L.S.L. and A.V.C. jointly identified the problem, performed the analysis and wrote the paper.

Additional information

The authors declare no competing financial interests. Supplementary information accompanies this paper on www.nature.com/naturephysics. Reprints and permissions information is available online at http://www.nature.com/reprints. Correspondence and requests for materials should be addressed to A.V.C.